Element-resolved magnetism across the temperature- and pressure-induced spin reorientation in MnBi

Yongseong Choi,[1] Xiujuan Jiang,[2] Wenli Bi,[1,3] Pavel Lapa,[4] Rajiv K. Chouhan,[5] D. Paudyal,[5] Tamas Varga,[6] Dmitry Popov,[7] Jun Cui,[2,5,8] Daniel Haskel,[1] and J. S. Jiang[4]

[1]*Advanced Photon Source, Argonne National Laboratory, Argonne, Illinois 60439, USA*

[2]*Energy and Environment Directorate, Pacific Northwest National Laboratory, Richland, Washington 99354, USA*

[3]*Department of Geology, University of Illinois at Urbana-Champaign, Urbana, Illinois 61801, USA*

[4]*Materials Science Division, Argonne National Laboratory, Argonne, Illinois 60439, USA*

[5]*Ames Laboratory, US Department of Energy, Ames, Iowa 50011, USA*

[6]*Environmental Molecular Sciences Laboratory, Pacific Northwest National Laboratory, Richland, Washington 99354, USA*

[7]*High Pressure Collaborative Access Team, Geophysical Laboratory, Carnegie Institution of Washington, Argonne, Illinois 60439, USA*

[8]*Materials Science and Engineering Department, Iowa State University, Ames, Iowa 50011, USA*

Rare-earth free permanent magnet MnBi (NiAs-type crystal structure) displays strong uniaxial magnetic anisotropy above its ∼90 K spin reorientation transition (SRT). X-ray magnetic circular dichroism (XMCD) measurements at the Mn K and Bi $L_{2,3}$ edges show induced magnetism in Bi, which is strongly coupled to the magnetism of Mn. Temperature- and pressure-dependent XMCD results reveal that hydrostatic pressure mimics the effect of temperature, driving a transition from uniaxial to in-plane anisotropy. The pressure and temperature transitions are shown to be connected to an anisotropic lattice contraction in NiAs-type structures. Temperature and pressure, hence, induce coupled structural and magnetic responses, highlighting the importance of both anisotropic lattice change and Mn-Bi hybridization in leading to the magnetic anisotropy change across the SRT. The dependence of magnetic anisotropy on the anisotropic lattice change is confirmed by density functional theory.

I. INTRODUCTION

The NiAs-type phase of MnBi has interesting properties such as high magnetic anisotropy and ferromagnetic ordering temperature above room temperature [1–3]. When increasing temperature above the spin reorientation transition (SRT) near 90 K, the magnetic easy axis direction changes from lying in the basal plane to along the c axis [Fig. 1(a)]. While magnetic anisotropy monotonically decreases with temperature in most ferromagnetic materials, the MnBi uniaxial anisotropy exhibits a peculiar increase with temperature up to 500 K [4]. The unusual magnetic anisotropy and the SRT make MnBi an attractive material both from a fundamental point of view as well as for high-temperature hard magnet applications.

Theoretical studies have shown that Bi-Mn hybridization leads to an induced moment on Bi [5–10]. In addition, the strong spin-orbit interaction on heavy Bi and related single-ion anisotropy likely plays a role in dictating the magnetocrystalline anisotropy energy (MAE) of MnBi [6]. This highlights the importance of an element-specific probe of electronic structure for a complete understanding of MnBi. A recent study has shown that the SRT is accompanied by a symmetry-lowering structural transition driven by exchange striction, emphasizing the importance of magnetostructural coupling [11]. This is also evident in pressure experiments where the SRT is tuned with applied pressure [12]. Theoretical and experimental studies have shown that the ratio between in-plane and out-of-plane lattice parameters plays an important role in determining the magnetic anisotropy and magnetization [11,13,14].

In Mn-pnictide ferromagnets, MnAs, MnSb, and MnBi, with hexagonal NiAs-type structures, structural response to temperature or pressure is characterized by anisotropic lattice change. A decrease in the c/a ratio can be induced by cooling in MnBi [11–13], and in MnSb and MnAs, it can be induced by hydrostatic or chemical pressure [15,16]. Decreasing temperature or increasing pressure leads to reduction in the c/a ratio in these isostructural magnets, and the magnetic transition in these materials is known to be sensitive to the anisotropic structural changes. Since the magnetocrystalline anisotropy energy is linked to orbital moment [17], it is worthwhile to investigate possible change in orbital moment across the SRT.

Here we used element-resolved x-ray magnetic circular dichroism (XMCD) to examine changes in Mn and Bi magnetism with both temperature and pressure. To date, element-resolved magnetic studies of MnBi have not been reported. As predicted by the theoretical studies, we observed induced magnetic moment on the Bi site. Furthermore, a significant change in Bi orbital-to-spin moment ratio, m_l/m_s, was found across the SRT. XMCD data indicate that applied pressure of less than 2 GPa can induce the SRT at room temperature. X-ray diffraction confirmed a reduction in c/a ratio with pressure. Density functional theory calculations indicate that the change in c/a ratio is linked to the magnetic anisotropy change from in-plane anisotropy to the uniaxial anisotropy.

II. METHODS

The polycrystalline powders of MnBi were synthesized by arc melting, grinding, heat treatment, and cryomilling. The XMCD and x-ray absorption spectroscopy (XAS) measurements were carried out at beamline 4-ID-D of the Advanced
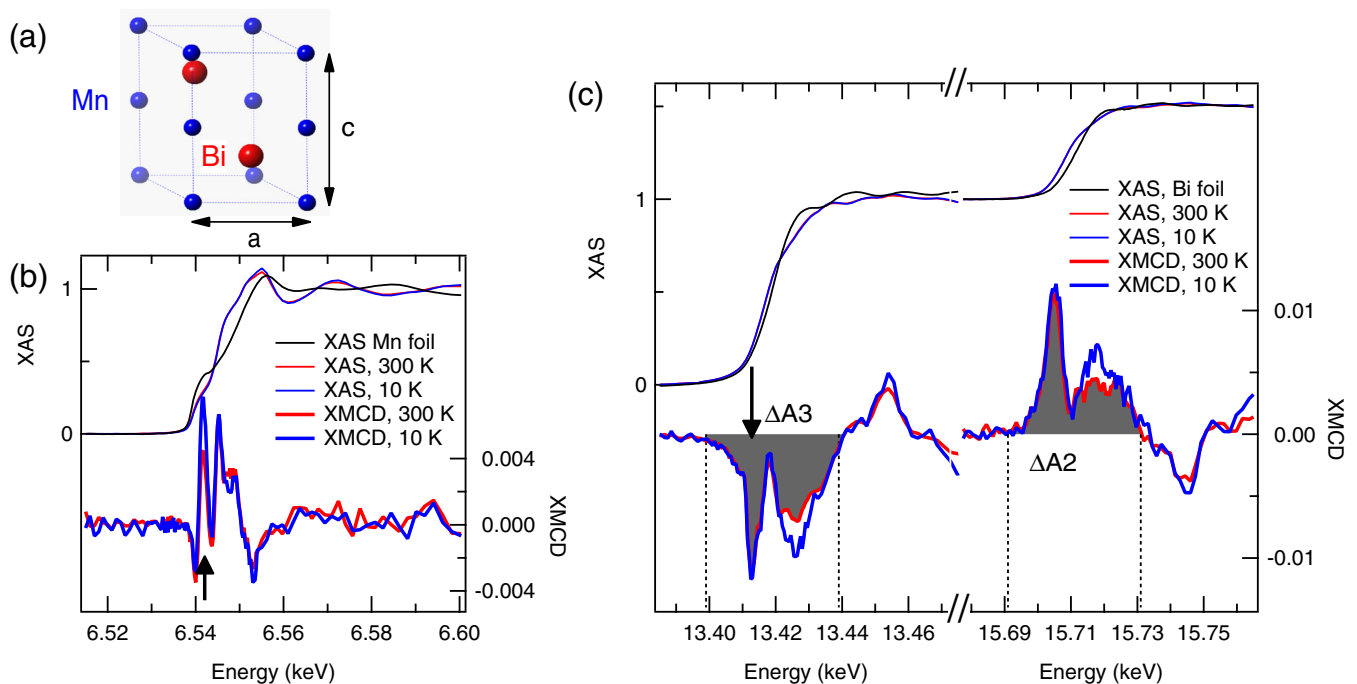
FIG. 1. (a) NiAs-type hexagonal crystal structure of MnBi. XMCD data at the (b) Mn K and (c) Bi L_3 and Bi L_2 edges, taken under a magnetic field of $+3.5$ T. XAS from reference Mn and Bi foils are also shown. Black arrows indicate x-ray energies used in field-dependent measurements, shown in Fig. 2. Vertical lines in (b) denote integration limits for sum rules. Ambient-pressure XAS/XMCD measurements (here and Fig. 2) were done on powders sandwiched between tapes.

Photon Source (APS), Argonne National Laboratory. At the Mn K ($1s \rightarrow 4p$ transition at 6.539 keV) and Bi $L_{2,3}$ ($2p \rightarrow 5d$ transition at 15.711 and 13.419 keV) edges, circularly polarized x rays were generated using 180 and 500 μm thick diamond (111) phase plates, respectively. The XMCD signal was measured by modulating x-ray polarization and detecting corresponding absorption modulation using a lock-in amplifier. The powder samples were measured in transmission mode with a magnetic field applied along the x-ray propagation direction.

To determine the XMCD sign, two reference samples, with well-known XMCD signs, were measured using the same experimental procedure (applied magnetic field direction and polarization switching) used for the Mn K and the Bi $L_{2,3}$ edges. XMCD spectra were taken at the Fe K from an Fe foil with the 180 μm thick diamond setup, and also the Ir L_3 XMCD from Sr_2IrO_4 powder with the 500 μm diamond setup. The Fe K and Ir L_3 XMCD signs were compared with the Mn and Bi $L_{2,3}$ XMCD signs in order to check the Mn and Bi XMCD signs.

Pressure dependence of MnBi magnetism was studied by monitoring the Bi $L_{2,3}$ XMCD signal at room temperature. Powder sample and ruby spheres were loaded with silicone oil as pressure medium in an Ar-filled glove box. The pressure study was carried out using two types of nonmagnetic diamond anvil cell (DAC) setups: pressure applied using a screw-type mini-DAC (D'anvils) that fits in the small bore of a 4 T superconducting magnet, and a membrane-driven CuBe DAC (easyLabs) that fits in the large bore of a 6.5 T superconducting magnet [18]. Pressure was calibrated using the ruby fluorescence method [19]. For ambient pressure measurements,

powder samples were prepared in an Ar-filled glove box by fixing between tapes and also in epoxy resin. The XMCD spectra from the powder fixed in epoxy show no discernible change relative to the data from powder on tapes, indicating no significant rotation of powders under high magnetic field in the latter samples. Pressure response of the MnBi structure was studied using powder diffraction at room temperature. Angle-resolved powder diffraction measurements with the incident energy 35 keV were taken at beamline 16-BM-D of APS. The powder samples were pressurized using a gasketed diamond anvil cell. Neon gas was used as hydrostatic pressure medium. Lattice parameters of hexagonal MnBi were determined from Rietveld refinements using the program TOPAS (version 5, Bruker AXS).

Density functional theory calculations were performed employing full-potential linearized augmented plane wave (FP-LAPW) method [20] with generalized gradient approximation (GGA) [21] including spin-orbit coupling (SOC) and on-site electron correlation (Hubbard U) parameter. The atomic radii for Mn and Bi are 2.5 and 2.7 atomic units, with plane wave cutoff parameters of $Rk_{max} = 9.0$ and $G_{max} = 14$, respectively. The k-space integrations have been performed with $20 \times 20 \times 12$ Brillouin zone mesh which was sufficient for the convergence of total energies (10^{-6} Ryd), charges, and magnetic moments.

III. RESULTS AND DISCUSSION

The Bi 5d states are nominally full, leading to the absence of unoccupied states with $d_{5/2}$ and $d_{3/2}$ character near the Fermi level and the absence of white line features in the

XAS of Bi $L_{2,3}$ edges. However, as seen in AuFe alloys [22], strong hybridization between s-p-d states can lead to a small fraction of unoccupied $5d$ states near the Fermi level in Au with nominally full $5d$ states. Unoccupied Bi $5d$ states arise via the same mechanism, and their polarization is probed by the L-edge XMCD measurements.

The MnBi sample undergoes a spin reorientation transition near 90 K. XAS and XMCD spectra below and above the transition are shown in Fig. 1. The Bi $L_{2,3}$ XAS and XMCD are normalized to a 1:0.5 L_3/L_2 edge jump ratio. The absence of white line features in the XAS spectra [23,24] indicates that oxidation of the powder is not significant. The Mn and Bi XAS spectra do not show noticeable changes across the transition. Recent studies indicate that anisotropic Bi atomic displacement [11] and Bi-Bi exchange striction [5] play important roles in the spin reorientation. The lack of changes observed in our XAS across the transition suggests that changes in the local environment around Mn and Bi are too subtle to be detected by XAS in powder samples.

The Mn K XMCD spectra in Fig. 1(b) have positive integrated areas, and the positive sign indicates that the $4p$ Mn orbital moment, induced by $3d$-$4p$ hybridization coupled with S-O interaction in the $4p$ band [25,26], is aligned against the field direction based on XMCD sum rules [27,28]. Considering the Mn $3d$ spin moment dominates the overall MnBi magnetization and aligns with the applied field, this result indicates that the Mn $4p$ orbital moment is antiparallel to the Mn $3d$ spin moment, in agreement with density functional theory [8,10]. An antiparallel alignment between Mn $3d$ spin and $4p$ orbital moments was also found by XMCD in GaMnAs [29,30].

The XMCD sum rules [27,28] can be used to get Bi $5d$ spin and orbital moments. In the current study, uncertainties in the number of Bi $5d$ holes and lack of clear XAS white line intensity make it difficult to quantify the individual spin ($m_s = -2\langle S_z\rangle$) and orbital ($m_l = -\langle L_z\rangle$) moments. Instead we focus on probing (the more reliable) changes in m_l/m_s. The XMCD sum rules give $\langle L_z\rangle = 2(\Delta A_3 + \Delta A_2)/C_0$ and $2\langle S_z\rangle + 7\langle T_z\rangle = 3(\Delta A_3 - 2\Delta A_2)/C_0$, where the terms $\Delta A_{3,2}$ are integrated $L_{3,2}$ XMCD areas, as shown in Fig. 1(b). The value C_0 is a positive value that depends on the XAS white line intensity and the number of Bi $5d$ holes. The $\langle T_z\rangle$ term is the magnetic dipole operator, which is a measure of the anisotropy of the spin density. This term cannot be readily measured experimentally but rather needs to be calculated from *ab initio* band-structure calculations. In $5d$ metal Pt (in Pt/Co film [31]) and Au (in AuFe alloy [22]), the $\langle T_z\rangle$ term is more than an order of magnitude smaller than the $\langle S_z\rangle$ term. Moreover, the x-ray absorption measurements are averaged over all crystallographic orientations in the powder samples studied here, and thus we neglected the $\langle T_z\rangle$ term in the sum rules.

From the XMCD data in Fig. 1(c) it is apparent that both $-2(\Delta A_3 + \Delta A_2)$ and $-3(\Delta A_3 - 2\Delta A_2)$ remain positive at 10 and 300 K, indicating that Bi $5d$ spin and orbital moments are aligned parallel to the field, hence parallel to the Mn $3d$ spin moment. Calculated values from the XMCD sum rules are shown in Table I. Electronic structure calculations have shown that strong interband interactions between Mn $3d$ and Bi $6p$ states can lead to induced Bi moments ($\sim 0.1\ \mu_B$/Bi)

TABLE I. Bi $5d$ orbital and spin moments (in arbitrary units) and their ratios, calculated from the Bi $L_{2,3}$ XMCD spectra.

Temperature (K)	m_l/C_0	m_s/C_0	m_l/m_s
10	6.0	158	0.038
300	6.7	135	0.050

antiparallel to the Mn moments [5–9]. Density of state calculations [6,8,10] also show that the Bi $6p$ and $5d$ moments are antiparallel. Thus, the observed parallel alignment between Bi $5d$ and Mn $3d$ moments is in agreement with the calculations. The parallel alignment of L and S in the Bi $5d$ band is as expected for a more than half-filled band. With increasing temperature, the Bi $5d$ orbital and spin moments change by $+12\%$ and -15%, respectively, resulting in a change in m_l/m_s of $\sim 30\%$. This correlates with the observed increase in MAE and decrease in saturation magnetization of MnBi seen across the SRT on warming ($m_l/m_s = 0.038$ at 10 K).

The field dependence of the XMCD asymmetry ratio $(\mu^+ - \mu^-)/(\mu^+ + \mu^-)$, where the $\mu^{+,-}$ are XAS for opposite helicities, is shown in Fig. 2. The Mn and Bi loops are taken at incident x-ray energies corresponding to maximum XMCD signals. In Fig. 2(a), the field dependence at 300 K for Mn and Bi shows a wide hysteresis loop with a coercive field about 1.0 tesla (T). The Mn and Bi loops nearly overlap indicating strong coupling between Mn and Bi moments. At 10 K (below the SRT) [Fig. 2(b)], the coercive field becomes negligible, consistent with easy-plane anisotropy. We note that there is a small difference in coercivity between the Mn and Bi loops in Fig. 2(a). With significantly different absorption lengths at the Mn K and Bi L edges, two separate powder samples were prepared and used for the Mn and Bi XMCD measurements. We speculate that the coercivity difference is caused by variations in grain orientation.

The effect of compressive stress on the magnetic response was studied with XMCD at the Bi L edges at 300 K, as shown in Fig. 3. While either temperature or pressure changes lead
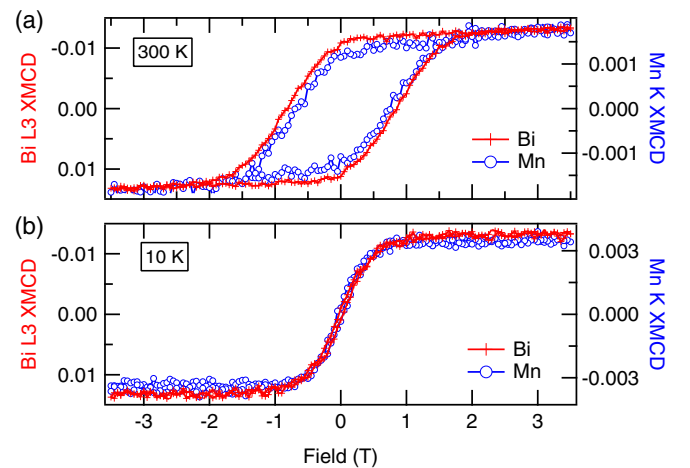

FIG. 2. Magnetic field dependence of the Mn K and Bi L_3 XMCD asymmetry ratio at (a) 300 K and (b) 10 K. The Mn data were taken at 6.542 keV and the Bi L_3 at 13.411 keV. Note that the left axis scales are reversed.
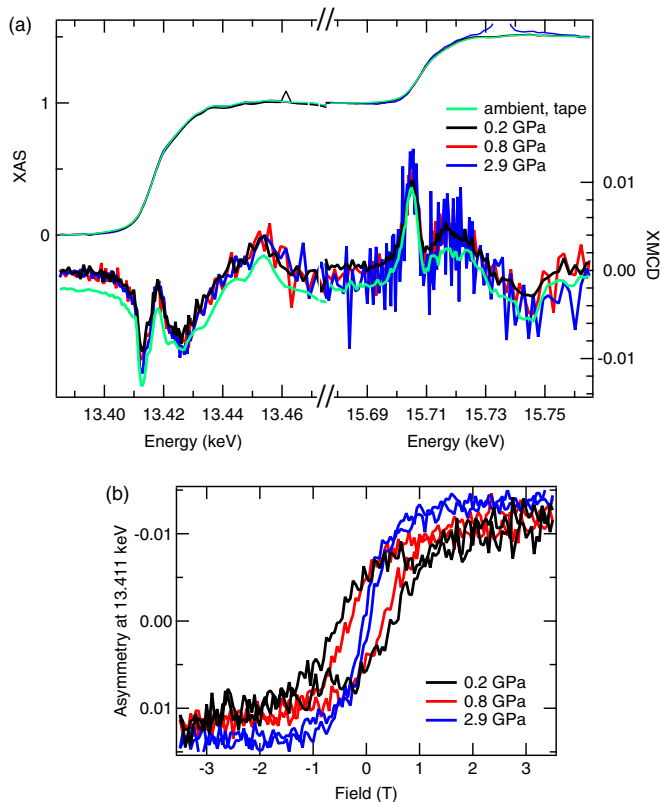
FIG. 3. (a) Pressure dependence of XMCD signals at the Bi L_3 and Bi L_2 edges at 300 K under +3.5 T field. The ambient-pressure XAS/XMCD spectra at 300 K from Fig. 1 were replotted for comparison. The ambient-pressure XMCD curves were shifted down for clarity. (b) Field dependence of Bi L_3 XMCD asymmetry ratio at selected pressures.

FIG. 4. (a) Bi L_3 XMCD spectra at selected pressures. (b) Magnetic field dependence of the Bi L_3 XMCD signal at selected pressures. Integrated area of the XMCD spectrum at each field is plotted. Loops are shifted vertically for clarity. All measurements were taken at 300 K. Arrow in (b) indicates the field sweeping direction.

to small changes in the XMCD spectra (Figs. 1 and 3), the noise level, likely related to smaller sampling volume inside the DAC, prevents us from calculating areas $\Delta A_{3,2}$ reliably. On the other hand, the field dependence of XMCD shows clear changes with pressure. Hysteresis loops, measured in the same way as the ambient-pressure data in Fig. 2, show a significant reduction in coercive field at 0.8 GPa and vanishing of coercivity at 2.9 GPa. As the pressure is released to 0.2 GPa the coercive field recovers, indicating that the pressure-induced change is reversible.

The loops shown in Figs. 2 and 3 were taken at a constant incident x-ray energy while changing field. A second set of pressure data was taken to check the Bi XMCD spectra at each pressure and field condition. Figure 4(a) shows Bi L_3 XMCD with +3.5 T at 300 K under several pressures. Figure 4(b) shows field-dependent XMCD intensity obtained by integrating the XMCD data (boundaries shown in the figure) at different pressures and fields. The coercive field becomes negligible as the pressure is increased from 1.2 to 1.7 GPa indicating that the pressure-induced magnetic transition is completed in this pressure range. The gradual change in the coercivity with pressure is consistent with the earlier studies showing the gradual reorientation of Mn moments with temperature across the SRT [13,32] and gradual change in the SRT with pressure [12].
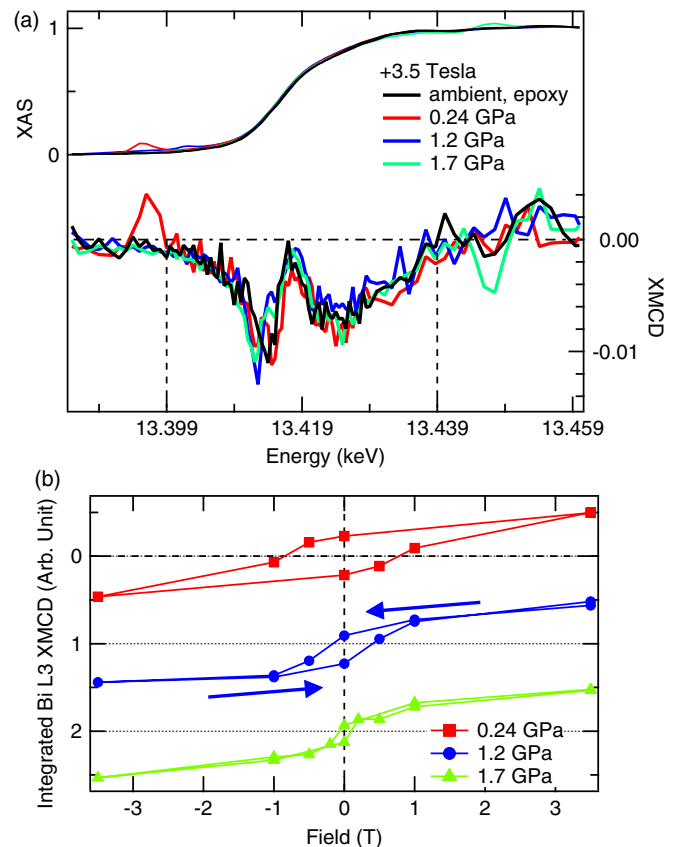
The temperature dependence of the in-plane and out-of-plane lattice parameters is known to show anisotropic changes [11–13]. With decreasing temperature the c/a ratio decreases in MnBi and other Mn-pnictide magnets. Here we studied the pressure dependence of the lattice parameters a and c of the hexagonal NiAs structure. Results of the powder diffraction measurements are summarized in Fig. 5. The rates of change with pressure are -0.013 and -0.043 Å/GPa for a and c, respectively. The c/a ratio in MnBi decreases with increasing pressure, and a similar pressure effect on the c/a ratio has been reported on isostructural MnSb [15]. Temperature and pressure effects have similar effects on the c/a ratio, which in turn can modify the magnetic transition.

In order to understand the interplay between anisotropic lattice contraction and magnetic anisotropy we carried out density functional theoretical calculations. We studied the magnetic anisotropy dependence on the c/a ratio using theoretical calculations. A high-resolution XRD experiment on a single crystal of MnBi [11] shows high-temperature hexagonal to low-temperature orthorhombic transformation in MnBi. Our calculations, however, were carried out within the hexagonal structure and focused instead on the importance of the c/a ratio on the magnetic anisotropy. We have used c/a ratios with corresponding lattice constants shown in Fig. 5 with
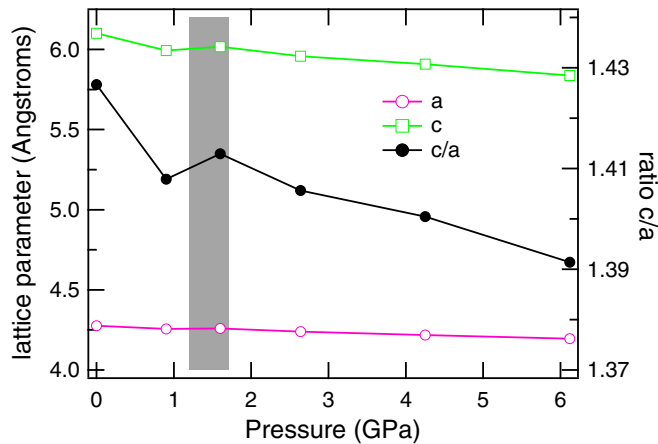
FIG. 5. The lattice parameters a and c and the c/a ratio at different pressures. Shaded area between 1.2 and 1.7 GPa denotes the SRT, identified from the pressure-dependent XMCD data in Fig. 4.

atomic positions Mn (0, 0, 0) and Bi (0.3333, 0.6667, 0.25) [33]. Here the magnetic anisotropy is calculated by taking the total energy difference between spin orientation along the c axis and in the ab plane.

The FP-LAPW calculations within GGA functional incorporating the Hubbard U parameter ($U = 4.0$ eV and $J = 0.97$ eV) and spin-orbit coupling (GGA+U+SOC) show that the maximum in-plane anisotropy (-0.78 meV/f.u.) is at $c/a = 1.407$. The in-plane anisotropy is favorable when the c/a ratio is low, and c-axis anisotropy becomes more favorable as the ratio increases (Fig. 6). The calculated c/a ratio for the SRT is about 1.45, slightly higher than the corresponding experimental value of 1.41 from Fig. 5. However, the overall pressure dependence shows the same trend in the calculated and experimental values. The observed trend is consistent with an earlier report, showing a sign change in MAE with increasing in-plane lattice parameter a [14], and the dependence of MAE on the c/a ratio provides an explanation for the similar effects on the magnetic anisotropy between pressure and temperature.

In isostructural and isoelectronic Mn-pnictide magnets, there is a link between the anisotropic structural change and magnetic transition [11–13,15,16]. For this apparent magnetostructur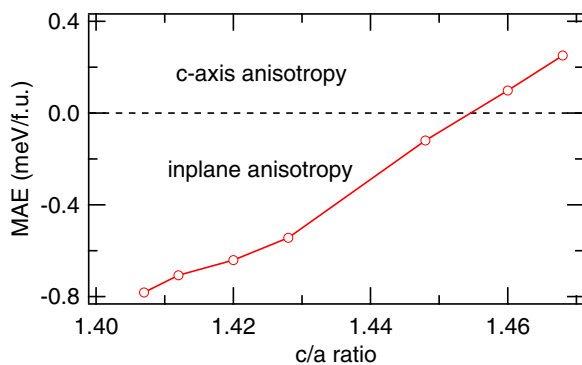al coupling, the dependence of the magnetic interaction on the Mn-Mn interatomic distance is known to play an important role. In addition, the strong hybridization between Mn-$3d$ and $3d^{10}4p^3$(As), $4d^{10}5p^3$(Sb), and $5d^{10}6p^3$(Bi) orbitals may provide another important link between structure and magnetism. The systematic increase in the magneto-optical effect, local Mn moment, and magnetic ordering temperature from MnAs to MnSb to MnBi points out the important role played by the pnictogen atoms [8]. In Mn-pnictide magnets, the hybridization with Mn similarly leads to induced moment in As, Sb, and Bi atoms that is antiparallel to the Mn $3d$ moment [8,34–36]. The magnetism in these Mn pnictides is dominated by the localized moments in Mn $3d$ orbitals. While the Mn $3d$ orbitals are more localized, these pnictogen p and d orbitals are less localized. Thus the delocalized nature of these pnictogen orbitals makes them sensitive to the structural distortions, and the strong overlap between the pnictogen p and Mn $3d$ orbitals may provide an additional link between structure and magnetism.

Recent theoretical studies have revealed the important role of Bi atoms in MnBi magnetism. Bi-Bi exchange interaction can be an important contributor to the anisotropy change [5]. In addition, lattice vibration may affect temperature dependence of the magnetic interactions among Mn and Bi sites and thus the magnetic anisotropy change [9]. A recent experimental result revealing concomitant changes in Bi vibrations and structural anisotropy with temperature [11] further supports the important role played by the Bi atoms in the magnetic anisotropy change.

In the present study, decreasing temperature and increasing pressure similarly cause reduction in coercivity. Increasing pressure leads to a reduction in the c/a ratio, and it has been reported that the c/a decreases with cooling [11–13]. The similar magnetic and structural responses to temperature and pressure suggest a close link between the anisotropic structural response and magnetic anisotropy changes. The coupling between structure and magnetism is further evidenced in a significant change in the L/S ratio accompanying the SRT.

The Bi $L_{2,3}$ XMCD measurements are sensitive to the Bi $5d$ orbitals. The Mn-Bi hybridization is identified as the origin of the magnetism in the Bi p and d orbitals [5]. While the overlap between Mn and Bi p states is more pronounced than that between Mn and Bi d states, the similar temperature and field dependencies of Mn- and Bi-specific hysteresis loops in Fig. 2 indicate that the Mn hybridization with the Bi $5d$, however smaller than the Mn-Bi $6p$ counterpart, is still sizable. In addition, while we only considered the $2p \rightarrow 5d$ dipole transition at the Bi $L_{2,3}$ edges, similar features noticeable between the calculated Bi p and d density of states [5,8] and the experimental XAS data suggest that the Bi $L_{2,3}$ data may contain some Bi $6p$ character. The link between magnetism and structure is further corroborated by theoretical calculations showing a strong dependence between lattice parameters and Mn-Bi hybridization [5] and a strong correlation between lattice parameters and magnetocrystalline anisotropy [14].

IV. SUMMARY AND CONCLUSIONS

In summary, we observed an induced Bi $5d$ magnetic moment whose orientation is parallel to the Mn $3d$ moment, in agreement with theoretical predictions. The induced Bi

FIG. 6. The magnetocrystalline anisotropy energy (MAE) as a function of ratio of lattice constants (c/a) within the hexagonal MnBi.

moment is strongly exchange coupled to the Mn moment and displays an orbital component, a result of spin-orbit coupling in heavy Bi atoms. Evidence for strong magnetostructural coupling is seen not only in the similar effects of cooling and compression on the SRT but also in the response of Bi orbital magnetism across this transition. Modest pressures below 2 GPa (20 kbar) induce the SRT at room temperature, in close agreement with $dT_{SRT}/dP = 9.6$ K/kbar reported in an earlier study [12]. The observed reduction of coercivity with cooling and compression suggests a transition from the *c*-axis uniaxial high magnetic anisotropy phase to the in-plane low-anisotropy phase. Taking into account the anisotropic lattice change with temperature or pressure and the gradual changes in magnetism induced by these external stimuli, the SRT transition appears to be a direct consequence of the structural distortion that upsets the subtle balance between the Mn-Bi interactions arising from the Mn-Bi hybridization and the Mn-Mn magnetic coupling. Density functional theory calculations lend support to the observed link between magnetic anisotropy and anisotropic lattice changes. Our results highlight opportunities for manipulating the anisotropy of MnBi with applied stress at room temperature, including at strained interfaces of thin-film heterostructures.

[1] R. R. Heikes, Phys. Rev. **99**, 446 (1955).

[2] B. W. Roberts, Phys. Rev. **104**, 607 (1956).

[3] T. Chen, J. Appl. Phys. **45**, 2358 (1974).

[4] T. Chen and W. Stutius, IEEE Trans. Magn. **10**, 581 (1974).

[5] V. P. Antropov, V. N. Antonov, L. V. Bekenov, A. Kutepov, and G. Kotliar, Phys. Rev. B **90**, 054404 (2014).

[6] R. Coehoorn and R. A. de Groot, J. Phys. F **15**, 2135 (1985).

[7] S. S. Jaswal, J. X. Shen, R. D. Kirby, and D. J. Sellmyer, J. Appl. Phys. **75**, 6346 (1994).

[8] P. Ravindran, A. Delin, P. James, B. Johansson, J. M. Wills, R. Ahuja, and O. Eriksson, Phys. Rev. B **59**, 15680 (1999).

[9] K. V. Shanavas, D. Parker, and D. J. Singh, Sci. Rep. **4**, 7222 (2014).

[10] J. B. Yang, W. B. Yelon, W. J. James, Q. Cai, M. Kornecki, S. Roy, N. Ali, and P. l'Heritier, J. Phys.: Condens. Matter **14**, 6509 (2002).

[11] M. A. McGuire, H. Cao, B. C. Chakoumakos, and B. C. Sales, Phys. Rev. B **90**, 174425 (2014).

[12] H. Yoshida, T. Shima, T. Takahashi, H. Fujimori, S. Abe, T. Kaneko, T. Kanomata, and T. Suzuki, J. Alloys Compd. **317-318**, 297 (2001).

[13] J. B. Yang, Y. B. Yang, X. G. Chen, X. B. Ma, J. Z. Han, Y. C. Yang, S. Guo, A. R. Yan, Q. Z. Huang, M. M. Wu, and D. F. Chen, Appl. Phys. Lett. **99**, 082505 (2011).

[14] N. A. Zarkevich, L.-L. Wang, and D. D. Johnson, APL Mater. **2**, 032103 (2014).

[15] H. Nagasaki, I. Wakabayashi, and S. Minomura, J. Phys. Chem. Solids **30**, 329 (1969).

[16] D. L. Rocco, A. de Campos, A. M. Carvalho, A. O. dos Santos, L. M. da Silva, S. Gama, M. S. da Luz, P. von Ranke, N. A. de Oliveira, A. A. Coelho, L. P. Cardoso, and J. A. Souza, Phys. Rev. B **93**, 054431 (2016).

[17] J. C. Slonczewski, Phys. Rev. **110**, 1341 (1958).

[18] D. Haskel, Y. Tseng, N. S. Neto, J. Lang, S. Sinogeikin, Y. Mudryk, K. A. Gschneider Jr., and V. Pecharsky, High Press. Res. **28**, 185 (2008).

[19] A. D. Chijioke, W. J. Nellis, A. Soldatov, and I. F. Silvera, J. Appl. Phys. **98**, 114905 (2005).

[20] P. Blaha, K. Schwarz, G. Madsen, D. Kvasnicka, and J. Luitz, *WIEN2k, An Augmented Plane Wave + Local Orbitals Program for Calculating Crystal Properties* (Karlheinz Schwarz, Techn. Universität Wien, Austria).

[21] J. P. Perdew, K. Burke, and M. Ernzerhof, Phys. Rev. Lett. **77**, 3865 (1996).

[22] F. Wilhelm, P. Poulopoulos, V. Kapaklis, J.-P. Kappler, N. Jaouen, A. Rogalev, A. N. Yaresko, and C. Politis, Phys. Rev. B **77**, 224414 (2008).

[23] N. Jiang and J. C. H. Spence, J. Phys.: Condens. Matter **18**, 8029 (2006).

[24] F. Farges, Phys. Rev. B **71**, 155109 (2005).

[25] J.-i. Igarashi and K. Hirai, Phys. Rev. B **50**, 17820 (1994).

[26] G. Schütz, W. Wagner, W. Wilhelm, P. Kienle, R. Zeller, R. Frahm, and G. Materlik, Phys. Rev. Lett. **58**, 737 (1987).

[27] B. T. Thole, P. Carra, F. Sette, and G. van der Laan, Phys. Rev. Lett. **68**, 1943 (1992).

[28] P. Carra, B. T. Thole, M. Altarelli, and X. Wang, Phys. Rev. Lett. **70**, 694 (1993).

[29] P. Wadley, A. A. Freeman, K. W. Edmonds, G. van der Laan, J. S. Chauhan, R. P. Campion, A. W. Rushforth, B. L. Gallagher, C. T. Foxon, F. Wilhelm, A. G. Smekhova, and A. Rogalev, Phys. Rev. B **81**, 235208 (2010).

[30] A. A. Freeman, K. W. Edmonds, G. van der Laan, R. P. Campion, A. W. Rushforth, N. R. S. Farley, T. K. Johal, C. T. Foxon, B. L. Gallagher, A. Rogalev, and F. Wilhelm, Phys. Rev. B **77**, 073304 (2008).

[31] M. Suzuki, H. Muraoka, Y. Inaba, H. Miyagawa, N. Kawamura, T. Shimatsu, H. Maruyama, N. Ishimatsu, Y. Isohama, and Y. Sonobe, Phys. Rev. B **72**, 054430 (2005).

[32] J. B. Yang, K. Kamaraju, W. B. Yelon, W. J. James, Q. Cai, and A. Bollero, Appl. Phys. Lett. **79**, 1846 (2001).

[33] J. Cui, J. P. Choi, G. Li, E. Polikarpov, J. Darsell, M. J. Kramer, N. A. Zarkevich, L. L. Wang, D. D. Johnson, M. Marinescu,

Q. Z. Huang, H. Wu, N. V. Vuong, and J. P. Liu, J. Appl. Phys. **115**, 17A743 (2014).

[34] R. Coehoorn, C. Haas, and R. A. de Groot, Phys. Rev. B **31**, 1980 (1985).

[35] A. Continenza, S. Picozzi, W. T. Geng, and A. J. Freeman, Phys. Rev. B **64**, 085204 (2001).

[36] M.-F. Li, T. Ariizumi, K. Koyanagi, and S. Suzuki, Jpn. J. Appl. Phys. **46**, 3455 (2007).